American Mineralogist, Volume 70, pages 106–123, 1985

High resolution solid-state sodium-23, aluminum-27, and silicon-29 nuclear magnetic resonance spectroscopic reconnaissance of alkali and plagioclase feldspars

R. James Kirkpatrick

Department of Geology
University of Illinois at Urbana-Champaign
1301 West Green Street, Urbana, Illinois 61801

Robert A. Kinsey, Karen Ann Smith

School of Chemical Sciences
University of Illinois at Urbana-Champaign
505 South Mathews Avenue, Urbana, Illinois 61801

Donald M. Henderson

Department of Geology
University of Illinois at Urbana-Champaign
1301 West Green Street, Urbana, Illinois 61801

and Eric Oldfield

School of Chemical Sciences
University of Illinois at Urbana-Champaign
505 South Mathews Avenue, Urbana, Illinois 61801

Abstract

We present in this paper high-resolution solid-state magic-angle sample spinning sodium-23, aluminum-27, and silicon-29 nuclear magnetic resonance (NMR) spectra of a variety of plagioclase and alkali feldspars and feldspar glasses. The results show that MASS NMR spectra contain a great deal of information about feldspar structures. In particular, we observe the following. (1) Al/Si order/disorder and exsolution effects in alkali feldspars are readily observable. (2) To our present level of understanding the published structure refinements of anorthite are not consistent with the NMR of spectra of anorthite. (3) The spectra of the intermediate plagioclases are interpretable in terms of *e*- and *I*-plagioclases, with much of the signal apparently coming from strained sites between albite-like and anorthite-like volumes in the *e*-plagioclases. (4) The nearest-neighbor atomic arrangements in albite and anorthite glasses are very similar to those in the corresponding crystals, although the range of cation–oxygen distances is larger in the glasses. (5) There are no aluminum-27 peaks in the range of 0 ppm that would indicate octahedrally coordinated aluminum in either glass.

Introduction

We present in this paper high-resolution solid-state sodium-23, aluminum-27, and silicon-29 nuclear magnetic resonance (NMR) spectroscopic results for a variety of plagioclase and alkali feldspars and feldspar glasses. The objective of this work is to explore the applicability of high-resolution solid-state NMR to the examination of the structures of complex silicate materials, such as feldspars and feldspar glasses. The emphasis in this paper is on the spectroscopic aspects of this problem. Future work will examine the mineralogical and petrological applications in more detail. Both magic-angle sample spinning (MASS) and variable-angle sample spinning (VASS) techniques have been used.

The samples discussed here include low albite, microline perthite, cryptoperthite, sanidine, a range of plagioclase compositions, and albite and anorthite glasses. The feldspar samples are listed in Table 1.

In this paper we briefly summarize feldspar nomencla-

0003–004X/85/0102–0106$02.00

Table 1. Silicon-29 NMR chemical shifts of feldspars and feldspar glasses

MATERIAL	LOCALITY	CHEMICAL SHIFT	COMMENTS
Albite (Ab99)	Amelia, Virginia	-92.2	T2m
		-96.3	T2o
		-104.4	T1m
Albite Glass (Ab100)	Synthetic	-98	broad peak
Sanidine (Or60Ab38An2)	Wyoming	-97	poorly separated
		-101	
Microcline Perthite	Deleware Co., Pennsylvania	-93	Ab T2m
		-96.0	T2m
		-98.6	T2o + Ab T2o
		-101.8	T1m
		-106.0	Ab T1m
Cryptoperthite (Spencer R) (Or43,Ab,53,An4)	"Fredriksvarn" (now Stavern, Norway)	-92.3	Ab T2m
		-96.0	Ab T2o + Or T2
		-98.0	Or T1
		-103.5	Ab T1m
Oligoclase (An23)	Bakersville, North Carolina	-87	Shoulder (An peak)
		-93.2	Ab peak
		-97.2	Ab peak
		-105.3	Ab peak
Labradorite (An52)	Sydney Mines, Labrador	-83	An peak
		-88	An peak
		-94	Ab peak
		-101	Ab peak
		-107	Ab peak
Bytownite (An70)	Crystal Bay, Minnesota	-84	Correlation to
		-89	Ab and An
		-95	peaks poor
		-101	
Anorthite (An92)	Pacaya Volcano Guatamala	-83.0	First two peaks
		-84.6	poorly resolved
		-89.2	
Anorthite (An100)	Synthetic	-82.9	Correlation to
		-84.8	published structure
		-89.6	refinements poor
Anorthite Glass (An100)	Synthetic	-87	broad peak

ture and structure and previous NMR work on feldspars, review the theory of MASS NMR (especially as it pertains to the study of quadrupolar nuclei), and present and discuss our results. These results are, we believe, only a beginning of the application of MASS NMR to feldspar mineralogy, and we present our conclusions with the recognition that they are in some instances tentative. It is clear from the work we have done, however, that MASS NMR spectra of alkali and plagioclase feldspars contain a great deal of information about Al/Si order/disorder in the tetrahedral sites, about chemical bonding in the sodium, aluminum and silicon sites, and also, we believe, about distortion of these sites due to exsolution. Our results indicate that solid-state MASS and VASS NMR, when combined with X-ray and electron diffraction and transmission electron microscopy (TEM) can provide new insights into the structures of a wide range of mineral phases.

Previous work

Feldspar structure and nomenclature

Feldspars are the most abundant minerals in the earth's crust and have received corresponding attention from mineralogists and petrologists. Excellent reviews of feldspar mineralogy are given in the compendia of Smith (1974) and Ribbe et al. (1983).

For the benefit of those unfamiliar with the feldspars, we summarize their main features (following Smith, 1974 and Ribbe et al., 1983), state some of our assumptions, and define some of our nomenclature and symbolism.

1. Feldspar structures are based on a framework of corner-linked SiO_4 and AlO_4 tetrahedra. The ratio of aluminum to silicon ranges from 1:3 to 1:1. We use the notation Q^4(nAl) to describe the *silicon* sites, where the superscript indicates the four bridging oxygen atoms and the integer n (0 to 4) denotes the number of aluminum (AlO_4) tetrahedra to which a silicon (SiO_4) tetrahedron is connected.

We assume, as is customary in dealing with tetrahedral silicon and aluminum occupancies, that the "aluminum avoidance rule" (Loewenstein, 1954; Goldsmith and Laves, 1955) holds for all feldspars. That is, no aluminum tetrahedron is linked to another aluminum tetrahedron, only to four silicon tetrahedra. *All* aluminum sites, therefore, should be A^4 (4Si). We will show, however, that for our synthetic anorthite this is not completely true.

2. Feldspar frameworks have inherent monoclinic or pseudomonoclinic symmetry. Because AlO_4 tetrahedra are slightly larger than SiO_4 tetrahedra, some patterns of Al/Si distribution give monoclinic frameworks, whereas others cause slight distortions and triclinic symmetry. The pattern of tetrahedral site occupancy leads to the important concept of Al/Si tetrahedral site order/disorder. Other things being equal, high Al/Si disorder promotes monoclinic frameworks, whereas increasing order promotes triclinic frameworks having increasing cell obliquity (indicated by the magnitude of the departure of the **B**-axis from **B***).

The large, irregular cages in the tetrahedral framework are occupied by potassium, sodium, or calcium ions. When occupied by the larger potassium ions, the cages are stretched and the framework tends to retain its monoclinic symmetry if it has a proper Al/Si distribution. If the Al/Si pattern is not appropriate, the symmetry is triclinic. When occupied by the smaller, sodium or calcium ions, the cages crumple a little and distort the framework slightly so that the symmetry is triclinic, regardless of the Al/Si order/disorder (except for the highest temperature sodium feldspar, monalbite).

3. Feldspar compositions are conveniently described in terms of percentages of the endmember *components* $KAlSi_3O_8$ (Orthoclase, Or), $NaAlSi_3O_8$ (Albite, Ab), and $CaAl_2Si_2O_8$ (Anorthite, An). The rock-forming feldspars occur in two series, the alkali feldspars (Or–Ab) and plagioclases (Ab–An).

4. The principal potassic feldspars include, from low to high temperature forms, microcline (triclinic, $C\bar{1}$), orthoclase or low sanidine (macroscopically monoclinic; monoclinic by polarized light microscopy but likely to be triclinic (low obliquity) by X-ray and electron diffraction), and high sanidine (monoclinic, $C2/m$). The principal sodic feldspars are low (temperature) albite and high albite, both triclinic, $C\bar{1}$; high albite has the lower cell obliquity. High sanidine and high albite form a continuous solid solution series despite their different symmetries.

5. In the triclinic alkali feldspars (microcline, low albite, high albite) there are four sets of similar but not identical tetrahedral sites conventionally labeled T1o, T1m, T2o, T2m. At high temperatures, the aluminum and silicon ions are randomly distributed over these sites. If a high temperature feldspar is quenched, this disorder is retained. In the lowest temperature

forms, maximum low albite and maximum microcline, Al/Si order is, ideally, complete, with all the aluminum in the T1o sites and all the silicon in the other three sites.

6. In the monoclinic alkali feldspars there are two sets of similar but not identical tetrahedral sites conventionally labeled T1 and T2. High sanidine ideally has one-quarter of an aluminum and three-quarters of a silicon in each site on the average (complete Al/Si disorder). Orthoclase (low sanidine) is more ordered, with equal numbers of aluminum and silicon atoms randomly occupying the T1 sites and silicon only occupying the T2 sites.

7. Non-endmember, single phase, high temperature alkali feldspars exsolve into intergrowths called perthites when cooled slowly enough. Cryptoperthite is perthite in which the intergrowth occurs on a submicroscopic scale. In the finer cryptoperthites, the lamellae of the potassium and sodium-rich phases are thought to maintain coherency across the interface causing strain of the sites near the interface. In the coarser perthites, microperthites and macroperthites, the boundaries between the lamellae are noncoherent, and there probably is no significant straining of the sites near the interfaces.

8. The plagioclases are even more complex. The albite endmembers have been described. The calcic endmembers are *P*-anorthite (triclinic, $P\bar{1}$) and *I*-anorthite (triclinic, $I\bar{1}$), which occur below and above 250°C, respectively. On cooling, the *I* to *P* transition is not quenchable. *P*- and *I*-anorthite have doubled *c* cell edge lengths of about 14Å compared to the 7Å of the other feldspars. Even the *P*-anorthite structure has a high degree of *I*-pseudosymmetry (Ribbe in Ribbe, 1983).

P-anorthite has 16 sets of similar but not identical tetrahedral sites. Eight are occupied by silicon and eight by aluminum. *I*-anorthite has 8 sets, four occupied by silicon and four by aluminum. Both kinds of anorthite ideally have complete Al/Si site order. Each silicon tetrahedron is connected to four aluminum tetrahedra, $Q^4(4Al)$, and vice versa, $A^4(4Si)$.

9. Standard compositional ranges of the plagioclases of intermediate compositions are labeled by the names oligoclase, An_{10-30}, andesine, An_{30-50}, labradorite, An_{50-70}, and bytownite, An_{70-90} (see Table 1). These names refer to bulk compositions, not phases. The intermediate plagioclases are all triclinic.

At the highest temperatures there is extensive solid solution between the Ab and An components. At lower temperatures, intermediate composition plagioclases exist as exceedingly fine intergrowths of albite-like and anorthite-like domains on several scales. The complexity of these plagioclases arises from the incompatibilities of the Al/Si site orderings in albite and anorthite and from the fact that subsolidus atomic rearrangement processes are so sluggish.

We shall accept the e-plagioclase model as described by Ribbe and by Smith in Ribbe (1983). The intergrowths in plagioclases occur on at least two scales. The finer type, *e*-plagioclase, is thought to consist of a modulated structure composed of coherent albite- and anorthite-like domains of the order of a few tens of Å across. *e*-plagioclase seems to be restricted to the range An_{20-70}.

A second category of intergrowth occurs on the micrometer scale and is associated with the so-called *peristerite* ($\sim An_{2-16}$), *Bøggild* ($\sim An_{47-58}$) and *Hüttenlocher* ($\sim An_{68-90}$) gaps. Peristerite intergrowths are considered here to be composed of albite ($\sim$An2) and an *e*-plagioclase ($\sim An_{25}$). Bøggild ones are believed to be composed of two *e*-plagioclases ($\sim An_{42}$ and $\sim_{56}$) and Hüttenlocher intergrowths are thought to be composed of an *e*-plagioclase ($\sim An_{68}$) and *I*-anorthite ($\sim An_{90}$). This *I*-anorthite is a type that *appears* to be body centered by diffraction, even at room temperatures. It is considered to have a composite structure made from domains of *P*-anorthite. Adjacent domains are "out-of-step" to one another (antiphase domains) with respect to Al/Si ordering, which, coupled with the earlier mentioned *I*-pseudosymmetry of each domain, causes systematic diffraction absences. These diffraction absences give an apparent $I\bar{1}$ symmetry for the average structure.

NMR of feldspars

Feldspars have been investigated by single crystal sodium-23 and aluminum-27 wide-line NMR at low magnetic field strengths since the early 1960's. Brun et al. (1960), Hafner et al. (1962), and Hafner and Laves (1963) investigated alkali feldspars and were able to resolve separate peaks from different phases. Hafner and Hartmann (1964) determined electric quadrupole coupling constants of a variety of compositions. Staehli and Brinkmann (1974a,b) examined the aluminum-27 NMR of anorthite using wide-line methods and were able to separate the eight aluminum sites, determine that the *P* to *I* transition takes place between 220° and 250°C, and again measure the values of the electric quadrupole coupling constants. The quadrupole coupling constants of feldspars and many other minerals have been summarized by Ghose and Tsang (1973).

Silicon-29 chemical shifts obtained by high-resolution MASS NMR have been presented by Lippmaa et al.

Table 2. Average Si–O bond distances, total cation–oxygen bond strengths, and predicted silicon-29 chemical shifts for anorthite

Silicon Site	Si–O Å	Bond Strength Sum (V.U.)	SEC $\angle$Si-O-Si
	Megaw et al. (1962)		
T1(000)	1.613	8.058	-1.438
T1(00i)	1.616	8.083	-1.471
T1(mz0)	1.608	8.036	-1.271
T1(mzi)	1.626	7.990	-1.266
T2(0z0)	1.613	8.187	-1.447
T2(0zi)	1.610	8.264	-1.367
T2(m00)	1.602	8.151	-1.346
T2(m0i)	1.628	7.879	-1.469
	Wainwright and Starkey (1971)		
T1(000)	1.616	8.144	-1.444
T1(00i)	1.613	8.123	-1.243
T1(mz0)	1.613	8.143	-1.451
T1(mzi)	1.613	7.926	-1.268
T2(0z0)	1.617	8.154	-1.446
T2(0zi)	1.608	8.183	-1.357
T2(m00)	1.615	8.000	-1.362
T2(m0i)	1.614	8.086	-1.442
	Kalus (1978)		
T1(000)	1.618	8.146	-1.445
T1(00i)	1.613	8.130	-1.458
T1(mz0)	1.614	8.075	-1.252
T1(mzi)	1.613	7.939	-1.273
T2(0z0)	1.617	8.129	-1.460
T2(0zi)	1.613	8.143	-1.366
T2(m00)	1.614	8.009	-1.346
T3(m0i)	1.616	8.061	-1.445

(1980) for what they call anorthite, albite, sanidine, orthoclase, and adularia. They presented spectra for albite and sanidine, discussed structural interpretations, and proposed peak assignments for the albite peaks. Oldfield et al. (1983) have discussed the effects of iron impurities on the aluminum-27 and silicon-29 MASS NMR spectra of a variety of feldspars. K. A. Smith et al. (1983) have discussed silicon-29 MASS NMR spectroscopy of a number of silicates, including some feldspars. Recently, J. V. Smith et al. (1984) have presented high resolution silicon-29 MASS NMR data for alkali feldspars and discussed the peak assignments. Solid-state aluminum-27 and silicon-29 MASS NMR have probably found their most important application to date in the study of zeolite catalyst materials (e.g., Klinowski et al., 1982).

Experimental methods

Spectrometers

The spectra presented here were recorded using three "home-built" Fourier transform NMR spectrometers using the methods described by Meadows et al. (1982) and Smith et al. (1983). The three spectrometers are based on 3.52, 8.45, and 11.7 Tesla superconducting magnets and use Nicolet 1180 or 1280 computers for data acquisition. All are equipped with Andrew-Beams type magic-angle sample-spinning rotor assemblies (Andrew, 1971), which can also be used to obtain static (non-spinning) spectra. Chemical shifts are reported in ppm relative to 3M NaCl for sodium-23, in ppm relative to 1M $Al(H_2O)_6^{3+}$ for aluminum-27, and in ppm relative to tetramethylsilane for silicon-29. More positive chemical shifts correspond to decreased shielding.

Sample preparation and characterization

All samples were ground to a fine powder using an agate (SiO_2) pestle and mortar and were tightly packed into Delrin rotors. Most samples were pure minerals and were simply ground and run. Pacaya anorthite was purified by hand picking and magnetic separation. The Wyoming sanidine was purified by hand picking and shaking in water in a small mill to remove the soft matrix.

The anorthite glass was prepared from 99.999% pure SiO_2, $CaCO_3$, and Al_2O_3 by melting for about one hour at 1600°C, three times, with grinding in an agate mortar between meltings. Synthetic anorthite crystals were grown by crystallizing the glass at about 1500°C for about four hours and then quenching the crystals. The albite glass was prepared by the Corning Glass Technical Staffs Division of Corning Glass Company.

All samples were characterized by powder X-ray diffraction and optical microscopy.

Theoretical background

A useful introduction to NMR spectroscopy is given in the book by Farrar and Becker (1971). Magic-angle sample-spinning (MASS) in general, and silicon-29 MASS NMR spectroscopy in particular, have been discussed by Lippmaa et al. (1980) and by Smith et al. (1983). We note here only that a given nuclide ordinarily has different nuclear resonance frequencies in different kinds of sites, whether in different materials or in the same material, even if the sites are as similar to each other as the tetrahedral sites in feldspars. This is because they are shielded from the imposed magnetic field by slightly different electron distributions. Silicon-29 has a nuclear spin I = 1/2, and, as described elsewhere (Andrew, 1971; Smith et al., 1983), spinning of a powdered sample on an axis inclined at 54.7° to the applied magnetic field (the "magic-angle") at kilohertz frequencies greatly narrows the NMR peak breadth and increases resolution. This is due to an effective averaging of the nuclear dipolar and chemical shift anisotropy interactions. Thus, nonequivalent silicon sites in an ordered crystal each give a single narrow peak. Peaks for glasses and disordered crystals are generally broader, because a range of magnetically nonequivalent sites is present.

Sodium-23 and aluminum-27, unlike silicon-29, have spins I = 3/2 and 5/2 respectively and, therefore, exhibit quadrupolar behavior. Although MASS averages the first order quadrupole interaction, for sites with large electric field gradients (and thus large quadrupole interactions) second-order terms in the nuclear quadrupolar Hamiltonian, H_Q, become important, and may cause a significant linebroadening. Such effects have been discussed in detail by Abragam (1961), Kundla et al. (1981), Meadows et al. (1982), Ganapathy et al. (1982), and Schramm and Oldfield (1982). We review here those aspects of theory necessary to understand the spectra presented.

A nucleus of spin I has (2I + 1) different nuclear energy levels when placed in a magnetic field, as shown for silicon-29 (I = 1/2, two energy levels) and sodium-23 (I = 3/2, 4 energy levels) in Figures 1A and D. In NMR spectroscopy the energies (or frequencies) of the transitions (1/2, −1/2), (1/2, 3/2), etc. are measured. In the absence of any other magnetic interactions, only a single resonance frequency would be observed. However, in real samples, there are a variety of interactions which cause slight changes in these nuclear energy levels. For silicon-29 the main effect is due to an orientation-dependent shielding of the main magnetic field at the nucleus. This is called the chemical shift anisotropy (CSA) and yields a broad resonance in powdered samples (Fig. 1B). In MASS this interaction is effectively averaged by rapid sample rotation in a sample rotor spun by an air-bearing at frequencies, ν_r, typically from about 2,000 to 6,000 Hz. The result is a sharp-line spectrum with a centerband (CB, Fig. 1C) at the same frequency as in the absence of the CSA, together with a number of spinning sidebands (SSB), spaced at the spinning frequency (ν_r).

For quadrupolar nuclei (sodium-23, I = 3/2, aluminum-27, I = 5/2), there are a number of transitions. In general, the resonances of these quadrupolar nuclei in powders are broadened by the interaction of the nuclear electric quadrupole moment (eQ) with the electric field gradient at the nucleus (eq). This interaction is described in terms of the quadrupole coupling constant, e^2qQ/h. For sodium-23, the first order quadrupole interaction leads to two broad absorptions due to the satellite transitions (3/2, 1/2; −1/2, −3/2) together with a relatively sharp central reso-

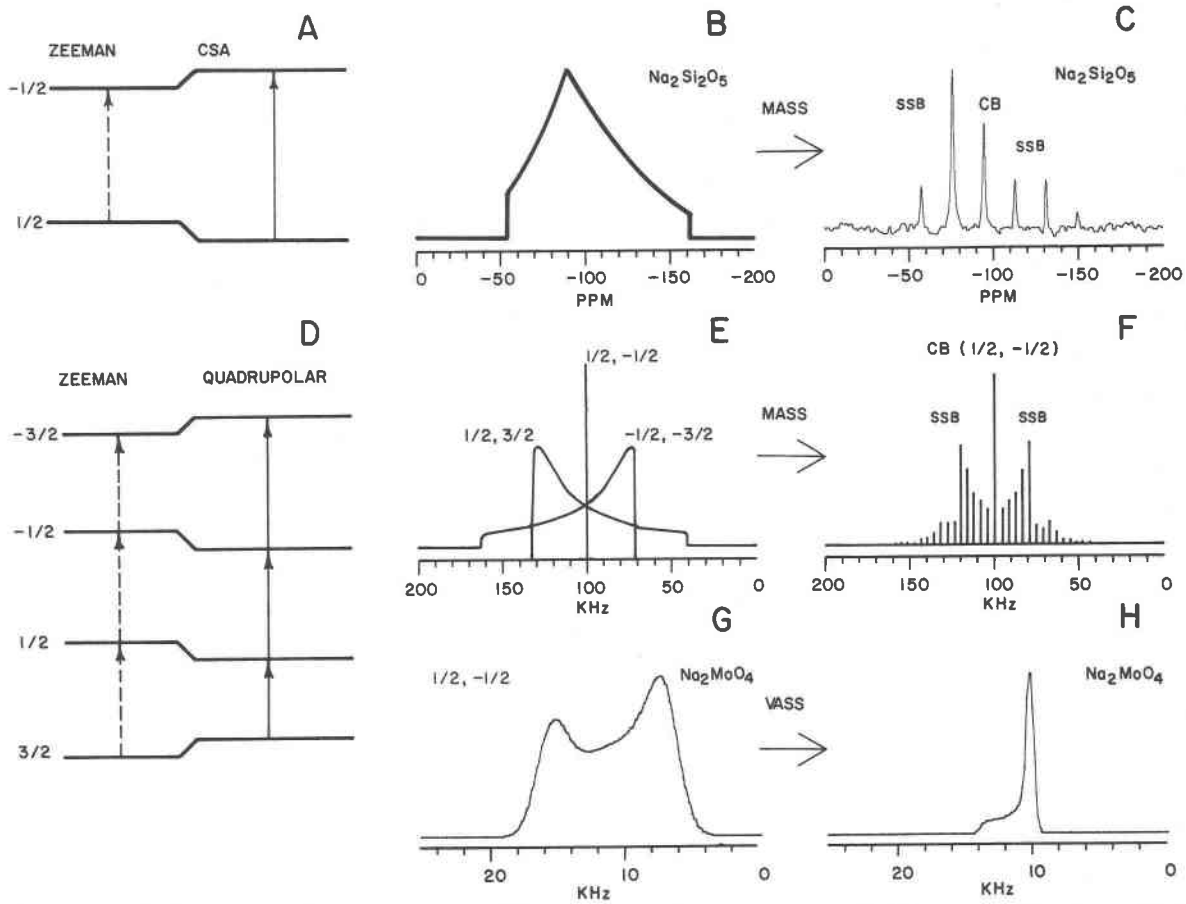

Fig. 1. Energy level diagrams, static spectra, and MASS NMR spectra of a spin I = 1/2 nuclide (A,B,C), a quadrupolar nuclide (spin I = 3/2) with a small quadrupole coupling constant (D,E,F), and a quadrupolar nuclide with a large quadrupole coupling constant (D,G,H). (A) Energy level diagram of spin I = 1/2 nuclide showing Zeeman splitting into 1/2, and −1/2 spin states and small additional splitting due to chemical shift anisotropy (CSA). (B) Simulation of a static spectrum of a spin I = 1/2 nuclide (silicon-29 in $Na_2Si_2O_5$) (C) MASS NMR spectrum of spin I = 1/2 nuclide (silicon-29) in $Na_2Si_2O_5$ showing the center band (CB, the true resonance) and spinning sidebands (SSB) spaced at the spinning speed, ν_r. (D) Energy level diagram of a spin I = 3/2 quadrupolar nucleus showing Zeeman splitting and a small additional splitting due to the quadrupolar interaction. (E) Simulation of a static spectrum of a quadrupolar nuclide (I = 3/2 in this case) which has a small quadrupole coupling constant. (F) Simulation of a MASS spectrum of an I = 3/2 nuclide showing the centerband (CB), which is the central (+1/2 → −1/2) transition and the spinning sidebands (SSB) mapping out the shape of the satellite spectra. (G) Simulation of the static spectrum of a quadrupolar nuclide with a large quadrupolar coupling constant (sodium-23 in Na_2MoO_4). Only the central (+1/2 → −1/2) transition is shown. (H) Simulation of the VASS NMR spectrum of sodium-23 in Na_2MoO_4 showing the narrowing possible at 75°. The MASS spectrum of this compound shows less narrowing.

nance (1/2, −1/2), as shown in Figure 1E. In general, with MASS, these interactions are again averaged, and a sharper central line (1/2, −1/2) together with a number of sidebands due to the satellite transitions are observed, Figure 1F. When the quadrupole coupling constant is about 1 MHz in frequency units, only the central (1/2, −1/2) resonance is readily detected, since there is a large residual broadening of the satellite lines, due to small fluctuations around the magic-angle due to wobbling of the sample rotor.

When the quadrupole coupling constant is larger (greater than about 3 MHz), additional structure generally appears on the central line due to the higher order effects which arise when the quadrupole interaction is a significant fraction of the actual resonance frequency. For example, for $^{23}Na_2MoO_4$ the quadrupole coupling constant is approximately 2.6 MHz, and at all fields in the range 3.52 to 11.7 Tesla there is a so-called second-order broadening of the central transition, Figure 1G. This interaction has a different angular dependence than that causing the first order chemical shift or quadrupolar broadenings. In order to reduce this interaction it is

necessary to spin the sample at a different angle in the magnetic field (variable-angle sample-spinning, VASS, Ganapathy et al., 1982).

Thus, for silicon-29, or for quadrupolar nuclei in highly symmetric environments (where electric field gradients are small)—such as sodium-23 in NaCl, magic-angle (54.7°) sample-spinning yields the highest resolution spectra, Figures 1C and F. For quadrupolar nuclei in highly asymmetric sites, such as sodium-23 in Na_2MoO_4, variable-angle spinning, at 75° in this case, yields the narrowest line width, Figure 1H. Both techniques are used here.

As discussed in detail elsewhere (Meadows et al., 1982), the second-order quadrupole interaction is a field-dependent interaction, and results in different apparent chemical shifts for different applied magnetic field strengths (Abragam, 1961). As a result, there may be significant discrepancies in the chemical shifts of a quadrupolar nucleus when results obtained at different magnetic field strengths are compared. All data for sodium-23 and aluminum-27 presented here were obtained at the three different magnetic field strengths to help determine the true chemical shifts. Because silicon-29 has spin I = 1/2, its chemical shifts are not field-dependent.

For the quadrupolar nuclei it is often useful to simulate (calculate) the spectra using the methods of Ganapathy et al. (1982). The parameters needed for the simulation are the quadrupole coupling constant (e^2qQ/h), the asymmetry parameter of the electric field gradient tensor (η), and the spinning angle (θ). The asymmetry parameter is a measure of the deviation of the electric field gradient at the nucleus from cylindrical symmetry (Abragam, 1961). Such simulations are used here in conjunction with published quadrupole coupling constants and asymmetry parameters to determine isotropic chemical shifts, and to look for contributions from exsolved phases.

For the silicon-29 NMR spectra we report the chemical shifts of narrow peaks to ±0.1 ppm, but subscript the last place because accuracy and reproducibility from laboratory to laboratory is probably only about 0.3 ppm. This is primarily due to magnet drift over the relatively long times (up to 12 hours) needed to collect some silicon-29 spectra. For broader silicon-29 peaks and shoulders we report the shifts to only ±1 ppm.

For the quadrupolar nuclei we report the values of most of the singularities or peak maxima to ±1 ppm. This is because even at 11.7 Tesla the peaks are at least 10 ppm wide. We report some of the narrowest singularities to ±0.1 ppm with the last place subscripted.

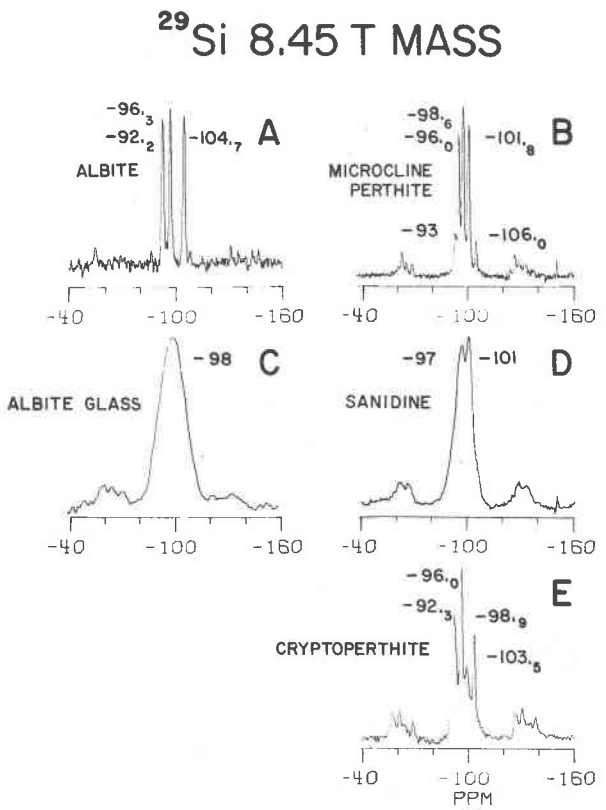

Fig. 2. 8.45 Tesla ^{29}Si NMR spectra (corresponding to a resonance frequency of 71.5 MHz) of natural alkali feldspars and a synthetic albite glass. (A) Albite (Amelia, Virginia), 2.4 kHz MASS, 31 scans at 600 sec recycle time, 8.6 kHz spectral width, 20 μsec 90° pulse excitation, 4096 data points, zero-filled to 8192, 25 Hz linebroadening due to exponential multiplication. (B) Microcline perthite (Delaware Co., Pennsylvania), 2.3 kHz MASS, 3000 scans at 10 sec recycle time, 8.6 kHz spectral width, 2.6 μsec 23° pulse excitation, 4096 data points, zero-filled to 8192, 5 Hz linebroadening due to exponential multiplication. (C) Synthetic albite glass, 2.4 kHz MASS, 87 scans at 600 sec recycle time, 8.6 kHz spectral width, 30 μsec 90° pulse excitation, 2048 data points, zero-filled to 8192, 100 Hz linebroadening due to exponential multiplication. (D) Sanidine (Wyoming), 2.4 kHz MASS, 2000 scans at 10 sec recycle time, 8.6 kHz spectral width, 2.6 μsec 23° pulse excitation, 4096 data points, zero-filled to 8192, 25 Hz linebroadening due to exponential multiplication. (E) Cryptoperthite ("Fredriksvarn", Norway), 2.7 kHz MASS, 65 scans at 600 sec recycle time, 8.6 kHz spectral width, 22 μsec 90° pulse excitation, 2048 data points, zero-filled to 8192, 25 Hz linebroadening due to exponential multiplication.

Results and discussion

Silicon-29

We present in Figures 2 and 3 the silicon-29 MASS NMR spectra of some representative feldspars and feldspar glasses obtained at a magnetic field strength of 8.45 Tesla. Table 1 summarizes the chemical shifts obtained from these spectra, together with sample locality and composition.

The spectra of all the crystalline samples contain considerable structure arising from silicon sites with different electronic environments. The spectra of albite and anorthite glass are both broad, single peaks with

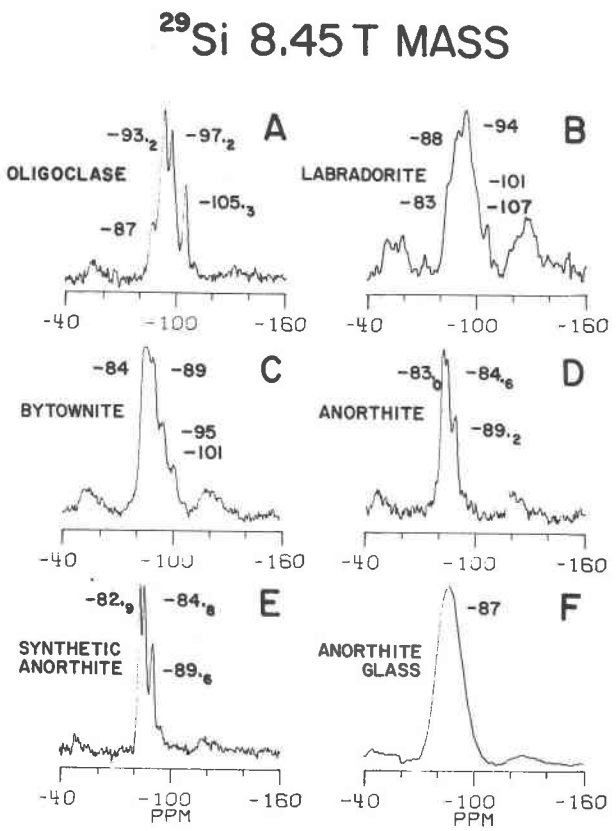

Fig. 3. 8.45 Tesla ^{29}Si MASS NMR spectra (corresponding to a resonance frequency of 71.5 MHz) of natural and synthetic plagioclase feldspars and a synthetic glass. (A) Oligoclase (Bakersville, North Carolina), 2.7 kHz MASS, 82 scans at 300 sec recycle time, 8.6 kHz spectral width, 30 μsec 90° pulse excitation, 2048 data points, zero-filled to 8192, 25 Hz linebroadening due to exponential multiplication. (B) Labradorite (Sydney Mines, Labrador), 2.4 kHz MASS, 52 scans at 600 sec recycle time, 8.6 kHz spectral width, 9 μsec 90° pulse excitation, 4096 data points, zero-filled to 8192, 75 Hz linebroadening due to exponential multiplication. (C) Bytownite (Crystal Bay, Minnesota), 2.3 kHz MASS, 313 scans at 8.6 sec recycle time, 10 kHz spectral width, 2.3 μsec 23° pulse excitation, 4096 data points, zero-filled to 8192, 25 Hz linebroadening due to exponential multiplication. (D) Anorthite (Pacaya Volcano, Guatamala), 2.7 kHz MASS, 64 scans at 600 sec recycle time, 8.6 kHz spectral width, 22 μsec 90° pulse excitation, 2048 data points, zero-filled to 8192, 25 Hz linebroadening due to exponential multiplication. (E) Synthetic anorthite, 2.5 kHz MASS, 31 scans at 600 sec recycle time, 8.6 kHz spectral width, 25 μsec 90° pulse excitation, 2048 data points, zero-filled to 8192, 25 Hz linebroadening due to exponential multiplication. (F) Synthetic anorthite glass, 2.4 kHz MASS, 91 scans at 600 sec recycle time, 8.6 kHz spectral width, 25 μsec 90° pulse excitation, 2048 data points, zero-filled to 8192, 100 Hz linebroadening due to exponential multiplication.

essentially no structure. Because silicon-29 has spin I = 1/2 and does not suffer from quadrupolar broadening, these broad, structureless peaks imply a continuum of electronic environments around the silicon sites. We first discuss the alkali feldspars whose spectra are shown in Figure 2.

The MASS NMR of low albite (Fig. 2A) was first examined by Lippmaa et al. (1980) and has also been discussed by K. A. Smith et al. (1983) and J. V. Smith et al. (1984). Because low albite has three particularly well resolved peaks, it has become a standard material in many NMR laboratories. The assignments of the three peaks to the three silicon sites in albite (Harlow and Brown, 1980) listed in Table 1 are those of Lippmaa et al. (1980), based on qualitative arguments, and elaborated by K. A. Smith et al. (1983), based on a procedure that uses cation-oxygen bond strength. The peak at −92.2 ppm is assigned to T2m, which has two aluminum next-nearest neighbors and two silicon next-nearest neighbors, Q^4 (2A1), and those at −96.3 and −104.7 ppm to T2o and T1m, which are Q^4 (1A1) sites. These assignments are the same as those of J. V. Smith et al. (1984) based on the mean secant of the Si–O–T angle.

The silicon-29 NMR spectrum of microcline perthite (Fig. 2B) exhibits five resolved peaks. The sample is a typical microcline perthite from a pegmatite. The microcline phase has a 131–$1\bar{3}1$ powder X-ray peak separation of −0.78° (Cu$K\alpha$) and is a maximum microcline. Our site assignments are based on the NMR measurements of cation-exchanged feldspars by J. V. Smith et al. (1984), which are different from those of K. A. Smith et al. (1983) based on the structure refinement of Brown and Bailey (1964). The new assignments of J. V. Smith et al. give the same order of peaks as for low albite. We assign the peaks at −96.0, −98.6 and −101.8 ppm in Figure 2B to T2m, T2o and T1m, respectively, of maximum microcline. The small peak at −93, the added intensity under the peaks at −96.0 and −98.6 ppm and the small peak at −106.0 ppm belong to the small amount of intergrown low albite in the perthites.

The spectra of low albite and microcline perthite clearly demonstrate the high degree of Si/Al tetrahedral site ordering that has been deduced for these minerals by X-ray diffraction. The fact that there is no recognizable silicon-29 signal for the T1o site in either spectrum is also consistent with the accepted models for these minerals which propose that T1o is occupied entirely by aluminum.

The spectrum of cryptoperthite in Figure 2E has some similarities to those of albite and microcline perthite. There are four resolved peaks, but the background under these peaks is higher than for the other two minerals.

This cryptoperthite comes from "Fredriksvarn" (now Stavern) in the well known Larvik region in southern Norway. Many of the cryptoperthites from this region are moonstones. Our sample is the much-studied "Spencer R" (Spencer, 1937). The cryptoperthites from the Larvik region are highly sodic, vary from place to place and are likely to be zoned compositionally and texturally (Spencer, 1937; Oftedahl, 1948; Muir and Smith, 1956; Smith and Muir, 1958). Spencer R has a bulk composition (mole percent) of about $Or_{43}Ab_{53}An_4$ (Spencer, 1937). The

aggregate perthite of our sample has monoclinic optics. Albite exsolution lamellae, though very fine, are clearly visible under the polarizing microscope, even at low magnifications. Nonetheless, transmission electron micrographs of Spencer R (e.g. Bollmann and Nissen, 1968) show albite lamellae less than 1000Å across.

Stewart and Wright (1974) report the potassic phase of Spencer R to be monoclinic (orthoclase) by powder X-ray diffraction and to have a composition (mole percent) of Or_{82}. They also report it to have the second largest amount of "strain" (Δa) of any potassic feldspar for which they have data.

It is to be noted that even the alkali feldspars from the Larvik area have significant calcium contents ranging from around An_4 to at least An_{10} (Spencer, 1937; Oftedahl, 1948; Muir and Smith, 1956; Smith and Muir, 1958). Ribbe (1983, p. 243), for example, reports that the exsolved plagioclase lamellae in cryptoperthite from Larvik (presumed by us to be similar to Spencer R) have a composition in the range An_{15-18} (oligoclase). In line with the bulk composition $Or_{43}Ab_{53}An_4$ for Spencer R, transmission electron micrographs of this and similar perthites from the Larvik area show the cross-sectional area of the plagioclase lamellae to exceed slightly that of the orthoclase.

The NMR spectrum (Fig. 2E) of the cryptoperthite is dominated by sodic plagioclase peaks at −92.3, −96.0 and −103.5 ppm because of the high degree of exsolution and the high proportion of sodic feldspar. These peaks are almost identical to the ones for low albite in Figure 2A and 2B, despite the probably higher An content and higher temperature state of the plagioclase lamellae in Spencer R.

Only two peaks attributable to the potassic feldspar phase are apparent: the added height of the peak at −96.0 and the small peak at −98.9 ppm.

In monoclinic alkali feldspars (orthoclase and sanidine) there are two sets of tetrahedral sites, T1 and T2. In ideal orthoclase, the T1 sites are thought to be randomly populated by aluminum and silicon ions; the T2 sites are thought to contain only Si ions. Such a phase should exhibit two silicon-29 NMR peaks, the one corresponding to T2 having about twice the area of the one corresponding to T1. In ideal sanidine, on the other hand, the T1 and T2 sites are both thought to be randomly populated by one-quarter aluminum and three-quarters silicon, on the average. In this case, one expects two NMR peaks of about equal area.

Unfortunately, the unavoidable interference by the plagioclase peak at −96.0 ppm makes it difficult to estimate the relative areas of the two peaks for orthoclase at −96.0 and −98.9 ppm. We infer that the low peak at −98.9 is from the T1 site because such a site is more likely than a T2 site to resemble the T1m site of microcline having a peak at −101.8 ppm. The added height of the peak at −96.0 ppm, therefore, is assigned to the T2 site. This is close to the peak at −98.6 ppm (Fig. 2B) from the T2o site of microcline.

By qualitative comparison of the −92.3, −96.0, and −103.5 ppm peaks of Spencer R (Fig. 2E) with those for low albite in Figure 2A, we believe that the component of the peak at −96.0 ppm (Fig. 2E) contributed by the T2 site of orthoclase is appreciably larger than the peak at −98.9 ppm contributed by the T1 site. This is consistent with the characterization of the potassic phase of the cryptoperthite as orthoclase.

We chose this cryptoperthite for study partly because it is thought to represent a potassic feldspar having a large number of strained sites in the coherent boundary regions between lamellae (Stewart and Wright, 1974). We expected to observe considerably broadened NMR peaks arising from ranges of distorted silicon sites in these boundary regions. The individual peaks in the cryptoperthite spectrum are just as sharp and narrow as those for low albite and microcline perthite. The unresolved background in the cryptoperthite spectrum, however, is much larger. We interpret this background as signal arising from strained sites in coherent boundary regions. The signal in the narrow peaks is coming from the unstrained volumes away from the lamellae boundaries.

The silicon-29 NMR spectrum of sanidine (Fig. 2D) consists of a broad doublet. This feldspar ($Or_{60}Ab_{38}An_2$) occurs as clear, glassy, 1 to 5 mm phenocrysts in rhyolite from Wyoming. Our interpretation of the sanidine spectrum is the same as for the orthoclase in the cryptoperthite. The two overlapping peaks represent the two sets of tetrahedral sites, T1 and T2, which are the only two present in monoclinic alkali feldspars. We infer that the peak at −101 ppm for sanidine corresponds to the peak at −98.9 ppm for orthoclase and arises from the T1 site, and that the peak at −97 ppm in sanidine corresponds to the peak at −96.0 ppm for orthoclase and arises from T2. Again, this is consistent with the low albite and microcline data, for which T2m and T20 are less shielded (less negative) than T1m.

The peaks for sanidine are much broader than any of those discussed so far. Because silicon-29 has spin I = 1/2, there is no broadening from quadrupolar interactions. Moreover, there should be no peak broadening from field inhomogeneity because our magnetic field inhomogeneity is less than 1 ppm. Consequently, we interpret the peak broadening to arise from Al/Si disorder in the occupancy of the two tetrahedral sites. The apparently equal areas under the two overlapping peaks indicates an approximately equal distribution of silicon and aluminum between the T1 and T2 sites, as expected for a high sanidine. Because of this disorder, for each of these sites there are probably $Q^4(0A1)$, $Q^4(1A1)$, $Q^4(2A1)$, and $Q^4(3A1)$ sites for both T1 and T2. Because of the overlapping of the peaks from each of these eight sites, and because of K/Na disorder, they cannot be resolved. The wings in Figure 2D in the range of 105 and 88 ppm are probably due to $Q^4(0A1)$ and $Q^4(3A1)$ sites respectively. A significant concentration of $Q^4(4A1)$ sites would not be expected for a phase with a Si/Al ratio of 3/1 (Klinowski et al., 1982).

We consider now the silicon-29 spectra of our plagioclases (Fig. 3). We have already dealt with the most common Na endmember, low albite. We consider first the calcium end-member, anorthite, and then the intermediate plagioclases.

The spectrum (Fig. 3E) of the synthetic anorthite has three well resolved peaks: at −82.9, −84.8 and −89.6 ppm and a small peak at about 95 ppm.

The spectrum of the natural anorthite (An_{92}), Figure 3D, is essentially identical to that of the synthetic anorthite, except that the peaks at −83.0 and −84.6 ppm are not as well resolved in the natural sample. The intensity in the range of −95 ppm may be due to $Q^4(3A1)$ sites, although the signal intensity is at about the noise level.

Anorthite at room temperature ("*P*-anorthite") has eight nonequivalent Si sites (Megaw et al., 1962; Wainwright and Starkey, 1971; Staehli and Brinkmann, 1974a,b; Kalus, 1978). The peaks in the anorthite spectra can be assigned using a correlation between the secant of the mean Si–O–Al angle for each site and the silicon-29 chemical shifts, similar to those for the silica polymorphs and alkali feldspars developed by J. V. Smith and Blackwell (1983) and J. V. Smith et al. (1984). This correlation gives three clusters of points using all three available structure refinements (Megaw et al., 1962; Wainwright and Starkey, 1967; and Kalus, 1978), while the bond strength sum and mean Si–O bond distance correlations of K. A. Smith et al. (1983) and Higgins and Woessner (1982) do not. The only discrepancy is the reversal of T1(ooi) and T1(mzo) in the Wainwright and Starkey structure, probably due to a long Al–O distance for their refinement. The variations in the bond strength sum and bond distance are small (0.2 V.U. and 0.005Å, respectively), and the predicted values are in the range of $Q^4(4A1)$ sites (Lippmaa et al., 1981; K. A. Smith et al. (1983).

The small peak for the synthetic anorthite at about −95 ppm is probably due to $Q^4(3A1)$ sites, which indicate a lack of perfect Al/Si order in this rapidly crystallized sample. The poorer resolution of the peaks in the natural anorthite (An_{92}) is probably due to the albite component.

Many of the peaks of the spectra of the intermediate plagioclases in Figures 3A, 3B, and 3C can be assigned to silicon sites similar to those in albite or anorthite. For none of these samples, however, can all the peaks of both albite and anorthite be recognized. Consequently, a simple model involving only domains of albite and anorthite structures and compositions cannot account for the observed spectra. We can, however, account for the spectra in terms of the earlier-mentioned low albite, *e*-plagioclase and *I*-anorthite structures. We attribute much of the signal in each spectrum to sites in strained volumes in *e*-plagioclase.

The spectrum of oligoclase in Figure 3A has many similarities to that of albite (Fig. 2A). The principal differences are that the peaks at −93.2, −97.2, and −105.3 ppm for oligoclase are broader, overlap considerably more, and have different relative heights, and that there is a small peak at −87 ppm. Because the chemical shifts are identical to those of albite, we assign the peaks at −93.2, −97.2, −105.3 ppm to the T2m, T2o and T1m sites of albite. We believe the low peak at −87 ppm arises from $Q^4(4A1)$ sites like those in anorthite. W. -H. Yang (1984 personal communication) has found a very similar spectrum for an An_{28} plagioclase.

It is possible to interpret the oligoclase spectrum in terms of a single *e*-plagioclase of composition An_{23}, a composition between the peristerite and Bøggild gaps. McLaren (1974) gives transmission electron micrographs of an oligoclase from the same locality as ours which show cross-hatched lamellae having a spacing of about 100Å. This is about the right order of magnitude for the spacings (20Å) that Smith (1974) says are to be expected for the modulated structure of Ab-rich and An-rich domains in this compositional range.

We believe that the peak broadening and overlap and the extra intensity in the −90 to −100 ppm range come from a range of silicon site environments in strained regions between the Ab-rich and An-rich domains in the modulated structure. The fact that the cell volume of albite (660$Å^3$) is less than the comparable half-cell volume (670$Å^3$) of anorthite suggests that the bond angles are distorted and that the silicon tetrahedra of the albite domains may be slightly stretched whereas those of the anorthite domains may be slightly compressed in the strained volumes around the coherent boundaries. The longer Si–O bonds in the outer parts of the albite domains are related to decreased shielding and less negative chemical shifts. The shorter Si–O bonds in the anorthite are related to increased shielding and more negative chemical shifts. There are probable changes in T–O–T bond angles also. The spectrum for this composition, therefore, is albite-like because the "albite" domains are larger. Because of this the ratio of strained to unstrained volumes of the albite-like material is relatively low. Because the volume of An-rich domains is small, all or most of this material is strained. This accounts for the lack of anorthite signal in the −83 ppm range. In addition, there could be a significant number of $Q^4(3A1)$ sites along the boundaries between the domains contributing signal in the range −90 to −95 ppm.

The small peak at about −108 may be due to $Q^4(0A1)$ sites in the boundaries between domains or to quartz impurity, which was not detected optically or by X-ray.

The spectrum of labradorite (Fig. 3B) shows rather ill-defined peaks or shoulders at −94, −101, and −107 ppm which may be assignable to $Q^4(2A1)$ and $Q^4(1A1)$ albite-like sites, but more signal than the oligoclase at less negative chemical shifts, a poorly resolved peak at −88 ppm, and a shoulder at −83 ppm. The significant amount of signal near −83 ppm indicates that the most deshielded $Q^4(4A1)$ anorthite-like sites are present in this sample.

This labradorite (An_{52}) falls in the Bøggild compositional gap, and probably consists of two *e*-plagioclases. It seems likely that the albite-like peaks arise mostly from

$Q^4(1Al)$ and $Q^4(2Al)$ sites in albite-rich volumes in the more albite-rich *e*-plagioclase. As for the oligoclase, the extra peak height in the −93 to −100 ppm range probably comes from sites in the strained regions around the margins of the albite volumes. If the calcium-rich phase in this material is also an *e*-plagioclase, some contribution to the albite-like peaks must also come from albite volumes in this material. The intensity at less negative chemical shifts (the peak at −88 ppm and the shoulder at −83 ppm) comes from $Q^4(4Al)$ anorthite-like sites, which occur in both *e*-plagioclases. As for the oligoclase, some signal in the central part of the spectrum could be due to $Q^4(3Al)$ sites at the margins of albite and anorthite-rich volumes. The relatively shielded value of the peak at −107 probably indicates some contribution from $Q^4(0Al)$ sites.

The bytownite spectrum (Fig. 3C) shows poorly resolved peaks at −84 and −89 ppm assignable to $Q^4(4Al)$ anorthite-like sites, shoulders at −95 and −101 ppm assignable to $Q^4(2Al)$ and $Q^4(1Al)$ albite-like sites, and little signal in the range of −105 ppm, although there is a small shoulder that may be real.

This bytownite (An_{70}) probably consists of (volumes of) *I*-plagioclase and *e*-plagioclase. The $Q^4(4Al)$ sites, which we believe to cause the peaks at −84 and −89 ppm, are in both materials. The $Q^4(2Al)$ and $Q^4(1Al)$ sites are in only the *e*-plagioclase. It seems likely that no −105 ppm peak is present (or it is very small) because essentially all of the albite volume is strained, causing all of the silicon sites in the albite to become deshielded. The peak at −84 ppm is probably due to overlap of the −82.9 and −84.8 peak of pure anorthite.

The silicon-29 NMR spectra of the albite and anorthite glasses (Figs. 2C and 3F) consist of single broad peaks, with no apparent structure. They are each approximately 12 to 15 ppm broader than the total peak breadth of the corresponding crystalline phases. The peak for albite has a maximum at −98 ppm and covers the range from about −85 ppm to −115 ppm. The peak for anorthite has a maximum at −87 ppm and covers the range from about −72 to −105 ppm.

Assuming, as discussed below, that all the aluminum in these glasses is in tetrahedral coordination, both must have a fully polymerized framework structure. This is because the ratio of tetrahedral cations (Si + Al) to oxygen is 1/2. All the silicon sites must, therefore, be $Q^4(nAl)$. One question is what values does n have. W. -H. Yang (1984, personal communication) has examined the silicon-29 MASS NMR behavior of analbite produced by heating Amelia albite at 1073°C for 120 days and found that detectable amounts of $Q^4(3Al)$, $Q^4(2Al)$, $Q^4(1Al)$, and $Q^4(0Al)$ are present. The signal in this spectrum covers the range from −85 to −115 ppm. Because the spectrum of albite glass extends to even less shielded values, it seems likely that detectable amounts of all five possible types of silicon sites $Q^4(4Al)$ through $Q^4(0Al)$ are present in albite glass.

For anorthite glass the average silicon site must be $Q^4(4Al)$. Because of the range of sites in albite glass, it seems likely that a range of sites are present in anorthite also. This is consistent with the presence of $Q^4(3Al)$ sites in crystalline anorthite. Because the amount of signal in the silicon-29 spectrum of anorthite glass at values more shielded (more negative) than −100 ppm is small, the concentration of $Q^4(0Al)$ sites must be quite small. The presence of a significant amount of signal at values less shielded (less negative) than −80 ppm must be due to distorted $Q^4(4Al)$ sites. Some of these may be caused by the presence of Al in the second tetrahedral coordination shell. In perfectly ordered anorthite all of these would be occupied by Si, but in Al/Si disordered material some of these must be occupied by Al.

Aluminum-27

Figures 4 and 5 show the 11.7 Tesla aluminum-27 MASS NMR spectra of our samples. Table 3 lists the

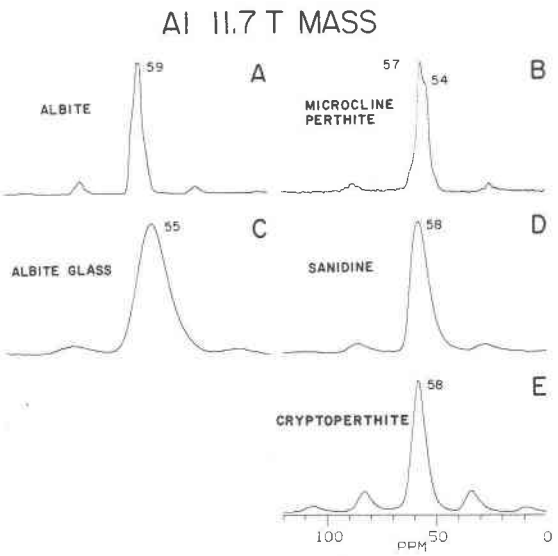

Fig. 4. 11.7 Tesla ^{27}Al MASS NMR spectra (corresponding to a resonance frequency of 130.3 MHz) of alkali feldspars and albite glass. (A) Albite (Amelia, Virginia), 3.5 kHz MASS, 10 scans at 25 sec recycle time, 15 kHz spectral width, 3 μsec 90° pulse excitation, 8192 data points, 10 Hz linebroadening due to exponential multiplication. (B) Microcline perthite (Delaware Co, Pennsylvania), 3.5 kHz MASS, 10 scans at 25 sec recycle time, 15 kHz spectral width, 3.5 μsec 90° pulse excitation, 8192 data points, 10 Hz linebroadening due to exponential multiplication. (C) Albite glass (synthetic), 5 kHz MASS, 200 scans at 1 sec recycle time, 15 kHz spectral width, 3 μsec 90° pulse excitation, 8192 data points, 50 Hz linebroadening due to exponential multiplication. (D) Sanidine (Wyoming), 3.2 kHz MASS, 158 scans at 25 sec recycle time, 15 kHz spectral width, 3.5 μsec 90° pulse excitation, 4096 data points, 50 Hz linebroadening due to exponential multiplication. (E) Cryptoperthite ("Fredriksvarn", Norway), 3.2 kHz MASS, 76 scans at 5 sec recycle time, 15 kHz spectral width, 4 μsec 90° pulse excitation, 4096 data points, 50 Hz linebroadening due to exponential multiplication.

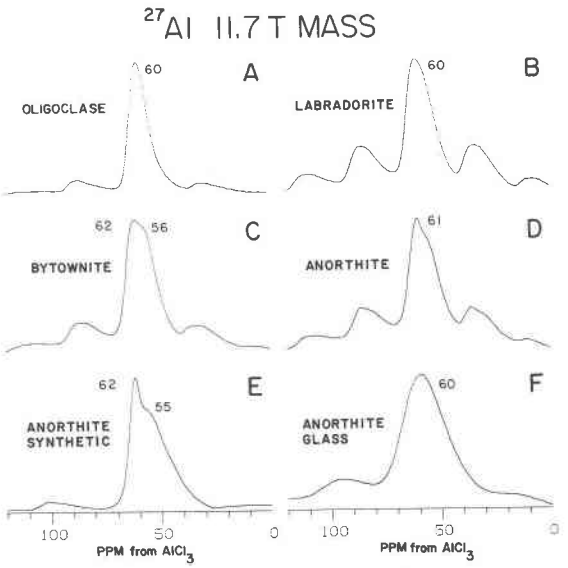

Fig. 5. 11.7 Tesla ^{27}Al MASS NMR spectra (corresponding to a resonance frequency of 130.3 MHz) of natural and synthetic plagioclase feldspars and anorthite glass. (A) Oligoclase (Bakersville, North Carolina), 3.6 kHz MASS, 36 scans at 10 sec recycle time 15 kHz spectral width, 5 μsec 90° pulse excitation, 4096 data points, 50 Hz linebroadening due to exponential multiplication. (B) Labradorite (Sydney Mines, Labrador), 3.3 kHz MASS, 1065 scans at 5 sec recycle time, 15 kHz spectral width, 4 μsec 90° pulse excitation, 4096 data points, 50 Hz linebroadening due to exponential multiplication. (C) Bytownite (Crystal Bay, Minnesota), 3.4 kHz MASS, 549 scans at 5 sec recycle time, 15 kHz spectral width, 4 μsec 90° pulse excitation, 4096 data points, 50 Hz linebroadening due to exponential multiplication. (D) Anorthite (Pacaya Volcano, Guatamala), 3.3 kHz MASS, 500 scans at 5 sec recycle time, 15 kHz spectral width, 4 μsec 90° pulse excitation, 4096 data points, 50 Hz linebroadening due to exponential multiplication. (E) Synthetic anorthite, 5.1 kHz MASS, 1300 scans at 10 sec recycle time, 15 kHz spectral width, 4 μsec 90° pulse excitation, 4096 data points, 50 Hz linebroadening due to exponential multiplication. (F) Synthetic anorthite glass, 4.9 kHz MASS, 1889 scans at 1 sec recycle time, 15 kHz spectral width, 4 μsec 90° pulse excitation, 4096 data points, 50 Hz linebroadening due to exponential multiplication.

observed chemical shifts. Aluminum-27 has spin 1 = 5/2 and, therefore, the aluminum-27 NMR spectra are affected by peak broadening and frequency shifts due to quadrupole interactions as discussed above. This quadrupolar broadening prevents us from obtaining as much detailed structural information as with silicon-29. All of the observed aluminum-27 chemical shifts are consistent with aluminum in four-fold coordination (Müller et al., 1981; Fyfe, et al., 1982).

We consider first the aluminum-27 NMR spectra of the alkali feldspars (Fig. 4). The spectrum for low albite (Fig. 4A) consists of a single asymmetric peak with a maximum at 59.3 ppm and a full-width at half-height of about 8 ppm. We assign this peak to the T1o site.

Figure 6 shows observed and simulated aluminum-27 and static and MASS NMR spectra for albite at 11.7, 8.45, and 3.5 Tesla. The great narrowing of the spectra with increasing magnetic field strength demonstrates that the peak shape is dominated by the second-order quadrupole interaction. The resolution increases as the square of the field strength (Meadows et al., 1982). The simulations in Figure 6 are in very good agreement with the experimental spectra. These simulations assume one kind of aluminum tetrahedral site with a quadrupole coupling constant of 3.29 MHz and an asymmetry parameter of 0.62. These values are based upon and in good agreement with the earlier single crystal NMR measurements for albite by Hafner and Hartman (1964). The simulations yield an isotropic chemical shift of 62.7±0.3 ppm. This is in the range of chemical shifts expected for tetrahedral aluminum (Müller et al., 1981).

The spectrum of microcline perthite (Fig. 4B) consists of a doublet having maxima at 54.3 and 57.3 ppm. Single crystal aluminum-27 NMR studies by Hafner and Hartmann (1964) have shown that microcline has one type of aluminum with a quadrupole coupling constant of 3.27 MHz and an asymmetry parameter of 0.21. Figures 7C and E show the observed aluminum MASS NMR spectrum of microcline perthite and a simulation assuming the Hafner and Hartmann values. The agreement is not very good. There is additional intensity in the experimental spectrum around 60 ppm. We believe that this is due to aluminum in the exsolved albite. Figure 7D shows a two

Table 3. Aluminum-27 NMR chemical shifts of feldspars and feldspar glasses

MATERIAL	FIELD STRENGTH (TESLA)	APPARENT[1] CHEMICAL SHIFT
Albite (Ab99)	3.5	-28,2,20,53
	8.45	53,56
	11.7	59
Albite Glass (Ab100)	3.5	44
	8.45	54
	11.7	55
Sanidine (~Or60)	11.7	58
Microcline Perthite	8.45	50,55
	11.7	54,57
Cryptoperthite	11.7	58
Oligoclase (An23)	11.7	60
Labradorite (An52)	11.7	60
Bytownite (An70)	11.7	62,56
Anorthite (An92)	11.7	61,55
Anorthite (An100)	3.5	45
	8.45	58
	11.7	62,55
Anorthite Glass (An100)	3.5	55
	8.45	57
	11.7	60

[1] For quadrupolar nuclei apparent chemical shift changes with field strength. Value at 11.7 Tesla is essentially the true isotropic chemical shift.

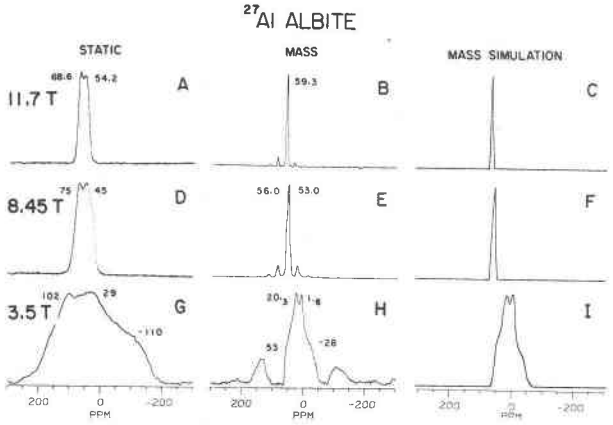

Fig. 6. ^{27}Al static and MASS NMR spectra of albite along with the MASS NMR computer simulations at 11.7, 8.45 and, 3.5 Tesla. (A) 11.7 Tesla, static, 30 scans at 25 sec recycle time, 78 kHz spectral width, 3 μsec 90° pulse excitation, 4096 data points, 50 Hz linebroadening due to exponential multiplication. (B) 11.7 Tesla, 4.0 kHz MASS, 10 scans at 25 sec recycle time, 78 kHz spectral width, 3 μsec 90° pulse excitation, 8196 data points, 10 Hz linebroadening due to exponential multiplication. (C) 11.7 Tesla, MASS simulation, 65 Hz linebroadening. (D) 8.45 Tesla, static, 50 scans at 25 sec recycle time, 56 kHz spectral width, 3 μsec 90° pulse excitation, 4096 data points, 50 Hz linebroadening due to exponential multiplication. (E) 8.45 Tesla, 4 kHz MASS, 50 scans at 25 sec recycle time, 56 kHz spectral width, 3 μsec 90° pulse excitation, 8196 data points, 10 Hz linebroadening due to exponential multiplication. (F) 8.45 Tesla, MASS simulation, 150 Hz linebroadening. (G) 3.5 Tesla, static, 300 scans at 5 sec recycle time, 24 kHz spectral width, 3 μsec 90° pulse excitation, 4096 data points, 100 Hz linebroadening due to exponential multiplication. (H) 3.5 Tesla, 4 kHz MASS, 300 scans at 5 sec recycle time, 24 kHz spectral width, 3 μsec 90° pulse excitation, 4096 data points, 100 Hz linebroadening due to exponential multiplication. (I) 3.5 Tesla, MASS simulation, 100 Hz linebroadening.

component simulation assuming 75% microcline and 25% albite. Figures 7A and B show the observed albite spectrum and a simulation at 11.7 T for comparison. The agreement between the two component simulations and the observed spectrum is excellent. The simulation (Fig. 7E) yields an isotropic chemical shift for microcline of 58.5±0.5 ppm. As for the albite, the aluminum-27 NMR data for microcline clearly indicate that essentially all the aluminum is in one tetrahedral site.

The spectrum for the cryptoperthite (Spencer R, Fig. 4E) consists of a single symmetric peak having a maximum at 57.9 ppm. As mentioned earlier, the bulk composition of this sample is about Or_{40}: there is a dominant oligoclase and a less abundant orthoclase. The quadrupolar broadening masks the splitting of the peaks from the Al sites in the orthoclase and oligoclase.

The spectrum of sanidine (Fig. 4D) is also a single symmetric peak, but is slightly broader than those of the other alkali feldspars (12 ppm wide at half-height). The maximum is at 58.5 ppm, intermediate between low albite and cryptoperthite. Single crystal NMR studies of sanidines (Brun et al., 1960) have not yielded discrete rotational patterns for different types of aluminum. The high resolution aluminum-27 MASS NMR lineshape of sanidine (Fig. 4D) agrees with this and is consistent with a range of quadrupole coupling constants, asymmetry parameters and/or isotropic chemical shifts. The H_o field dependence of the lineshape (data not shown) shows that the average quadrupole coupling constant is about 3 MHz, because the location and breadth of the centerband is similar to those of albite and microcline.

We consider now the aluminum-27 spectra of the plagioclases. The spectrum of synthetic anorthite (Fig. 5E) is more complicated that those of the alkali feldspars. It consists of a peak at 61.5 ppm and a broad shoulder at about 55 ppm, and is strongly asymmetric.

Anorthite at room temperature has eight slightly differ-

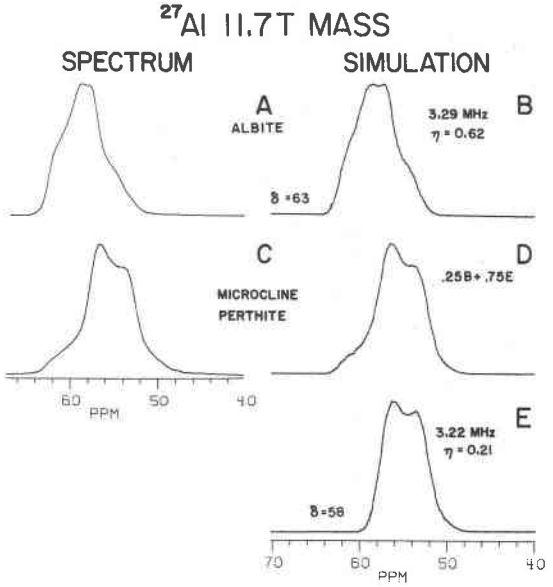

Fig. 7. 11.7 Tesla, ^{27}Al MASS spectra and computer simulations of albite and microcline perthite. (A) Albite, 4.0 kHz MASS, 10 scans at 25 sec recycle time, 4 kHz spectral width, 3 μsec 90° pulse excitation, 8196 data points, 10 Hz linebroadening due to exponential multiplication. (B) Albite, computer simulation using quadrupole coupling constant of 3.29 MHz and asymmetry parameter of 0.62, 65 Hz linebroadening. (C) Microcline perthite, 4.0 kHz MASS, 20 scans at 15 sec recycle time, 4 kHz spectral width, 3 μsec 90° pulse excitation, 8196 data points, 10 Hz linebroadening due to exponential multiplication. (D) Microcline perthite computer simulation using sum of albite simulation (B) and a second component having a 3.22 MHz quadrupole coupling constant and asymmetry parameter of 0.21, 75 Hz linebroadening due to exponential multiplication. (E) Computer simulation using 3.22 MHz quadrupole coupling constant and asymmetry parameter of 0.21 and 75 Hz linebroadening due to exponential multiplication.

ent aluminum tetrahedral sites. Single crystal NMR studies yield eight different electric field gradient tensors with quadrupole coupling constants ranging from 2.66 to 8.42 MHz (Staehli and Brinkmann, 1974a,b). The broadened peak in the MASS spectrum is due to overlap of the signals from the different Al sites.

The aluminum-27 spectra of the four natural, intermediate plagioclases (Figs. 5A, 5B, 5C, and 5D) all have peak maxima between 60.2 and 61.5 ppm. The peaks become broader and more like those of the synthetic anorthite with increasing An-content. Even for the Pacaya anorthite, the large peak and shoulder are less resolved than for the synthetic anorthite. The quadrupole broadening prevents resolution of the many closely spaced peaks.

The aluminum-27 NMR spectra of albite and anorthite glass (Figs. 4C and 5F) consist of broad, structureless peaks (about 18 and 28 ppm wide, respectively) with maxima at 55.0 and 59.6 ppm, respectively. Quantification of the total aluminum content in albite glass using the height of the free-induction decay yields about 75 percent of the expected intensity. Once again we interpret these spectra as indicating that the aluminum sites in the glass have a wide range of quadrupole coupling constants, asymmetry parameters, and/or isotropic chemical shifts.

The anorthite glass spectrum is skewed to less positive chemical shifts, with a very broad underlying component. Quantification of the aluminum indicates that only about 50% of the expected intensity is observed. As for the albite glass, we interpret this low intensity as indicating that the aluminum in the glass is in a wide range of electronic environments, many of which have large quadrupole coupling constants.

Little is known about the effects of Al–O bond distances or angles, total cation-oxygen bond strength, or other structural parameters on aluminum-27 chemical shifts and quadrupole coupling constants, so it is not possible at the present time to give a more detailed analysis of our results in structural terms. It seems likely, however, that at least part of the peak broadening is due to a wide range of electric field gradients around aluminum in the glasses. There is no signal in the chemical shift range near 0 ppm, which would indicate octahedrally-coordinated aluminum, although because we do not observe the full intensity expected on the basis of aluminum content, we cannot rule out the presence of highly distorted, six-coordinated sites. X-ray radial distribution studies (Taylor and Brown, 1979) and Raman spectroscopy (Mysen, et al., 1982) do, however, suggest that 6-coordinated aluminum is unlikely to be present in these glasses.

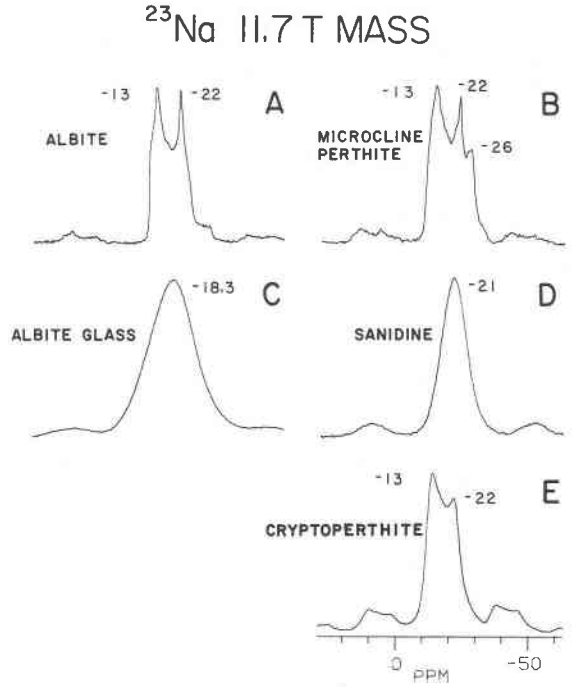

Fig. 8. ^{23}Na MASS NMR spectra of natural alkali feldspars and synthetic albite glass at 11.7 Tesla (coresponding to a resonance frequency of 132.3 MHz). (A) Albite (Amelia, Virginia), 4.0 kHz MASS, 30 scans at 25 sec recycle time, 15 kHz spectral width, 4 (μsec 90° pulse excitation, 8192 data points, 10 Hz linebroadening due to exponential multiplication. (B) Microcline perthite (Delaware Co., Pennsylvania), 4.0 kHz MASS, 100 scans at 25 sec recycle time, 15 kHz spectral width, 3 μsec 90° pulse excitation, 8192 data points, 10 Hz linebroadening due to exponential multiplication. (C) Albite glass (synthetic), 4.7 kHz MASS, 1003 scans at 1 sec recycle time, 15 kHz spectral width, 4 μsec 90° pulse excitation, 4096 data points, 150 Hz linebroadening due to exponential multiplication. (D) Sanidine (Wyoming), 4 kHz MASS, 159 scans at 5 sec recycle time, 15 kHz spectral width, 3.5 μsec 90° pulse excitation, 4096 data points, 50 Hz linebroadening due to exponential multiplication. (E) Cryptoperthite ("Fredriksvarn", Norway), 4 kHz MASS, 708 scans at 5 sec recycle time, 15 kHz spectral width, 4 μsec 90° pulse excitation, 4096 data points, 50 Hz linebroadening due to exponential multiplication.

Sodium-23

We show in Figures 8 and 9 the 11.7 T sodium-23 MASS NMR spectra for all of our sodium-containing samples. Table 4 lists the chemical shifts at the singularities. Sodium-23 has spin I = 3/2 and like aluminum-27 suffers from quadrupolar broadening. Because sodium-23 has a smaller nuclear spin than aluminum-27, for the same quadrupole coupling constant, sodium has a larger second-order quadrupole breadth and hence broader lines (Meadows et al., 1982).

The sodium-23 spectrum of low albite (Fig. 8A) consists of a doublet with peaks at −13.1 and −21.9 ppm. The split peak is *not* due to the presence of two sodium sites in albite, but is caused by the second order quadrupole interaction, which is only partially averaged by MASS. Single crystal sodium-23 NMR studies of low albite have yielded a quadrupole coupling constant of 2.62

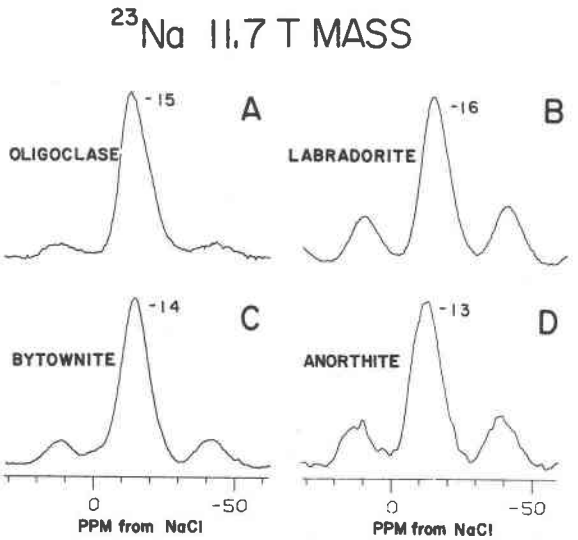

Fig. 9. ^{23}Na MASS NMR spectra of natural plagioclase feldspars at 11.7 Tesla (corresponding to a resonance frequency of 132.3 MHz). (A) Oligoclase (Bakersville, North Carolina), 3.6 kHz MASS, 118 scans at 10 sec recycle time, 15 kHz spectral width, 5 μsec 90° pulse excitation, 4096 data points, 50 Hz linebroadening due to exponential multiplication. (B) Labradorite (Sydney Mines, Labrador), 3.3 kHz MASS, 725 scans at 5 sec recycle time, 15 kHz spectral width, 4 μsec 90° pulse excitation, 4096 data points, 50 Hz linebroadening due to exponential multiplication. (C) Bytownite (Crystal Bay, Minnesota), 3.4 kHz MASS, 314 scans at 5 sec recycle time, 15 kHz spectral width, 4 μsec 90° pulse excitation, 4096 data points, 50 Hz linebroadening due to exponential multiplication. (D) Anorthite (Pacaya Volcano, Guatamala), 3.4 kHz MASS, 1000 scans at 5 sec recycle time, 15 kHz spectral width, 4 μsec 90° pulse excitation, 4096 data points, 100 Hz linebroadening due to exponential multiplication.

MHz and an asymmetry parameter of 0.25 (Hafner and Hartmann, 1964). The static and MASS lineshapes as a function of magnetic field strength (Fig. 10) are consistent with the lineshape being dominated by the quadrupole interaction. The 3.52 T MASS spectrum is very complex, containing many spinning sidebands, due to the fact that the spinning speed is much less than the spectral breadth, when expressed in frequency units.

We have obtained an excellent simulation of the 11.7 T MASS spectrum of albite (Fig. 11) assuming a single sodium site with a quadrupole coupling constant of 2.58 MHz and an asymmetry parameter of 0.25, and yielding an isotropic chemical shift of -6.8 ± 0.3 ppm, in good agreement with the value of -7.3 ppm obtained by Lippmaa et al. (1980). The agreement between the experimental and simulated spectra clearly indicates that there is only one sodium site in albite.

The values of the quadrupole coupling constant and asymmetry parameter of sodium-23 in albite are confirmed by variable angle sample-spinning (VASS) NMR, Figure 11, which generates different lineshapes depending on the spinning angle, when the second order quadrupole interaction dominates (Oldfield et al., 1983; Ganapathy et al., 1982). As expected, better averaging is obtained near 40° or 75°. Note that at 75° the first order spinning sidebands are absent (Ganapathy et al., 1982).

The sodium-23 spectrum of microcline perthite at 11.7 T (Fig. 8B) shows peaks at -13.1, -21.9 and -26.5 ppm. From the H_o magnetic field dependence of the lineshape (data not shown) there appear to be two types of sodium, one in exsolved low albite (-13.1 and -21.9 ppm) and one in microcline (-26.5 ppm). The -26.5 ppm line is not appreciably shifted in going from 8.45 T to 11.7 T, suggesting that the sodium site in microcline has a smaller electric field gradient and, hence, is in a more symmetric environment than in albite. Spectra of microcline obtained at 11.7 T simulate well with an albite component and an additional 10% contribution from a line with a quadrupole coupling constant of about 0.5 MHz, this additional intensity being from sodium in the microcline. The low quadrupole coupling constant is in agreement with the small magnetic field dependence of the chemical shift. However, because equally good spectral simulations can be obtained using two powder patterns having e^2qQ/h of about 3 MHz, further work is needed in order to substantiate this very tentative assignment.

The sodium-23 MASS NMR spectrum of the cryptoperthite (Fig. 8E) shows a doublet due to the second-order quadrupole interaction. These peaks are very similar to those of albite, except that they are less well resolved. This spectrum is in agreement with the silicon-29 and aluminum-27 data, which indicate that some Si/Al ordering has occurred in this material, but that neither is as complete as in low albite or microcline perthite.

Table 4. Sodium-23 NMR chemical shifts of feldspars and feldspar glasses

MATERIAL	FIELD STRENGTH (TESLA)	APPARENT[1] CHEMICAL SHIFT	COMMENTS
Albite (Ab99)	8.45	-18 -35	Quadrupole Split Peaks
	11.7	-13.1 -21.9	Quadrupole Split Peaks
Albite Glass (Ab100)	11.7	-18	
Sanidine (~Or60)	11.7	-21	
Microcline Perthite	11.7	-13 -22 -26	Na-rich phase Na-rich phase K-rich phase
Cryptoperthite	11.7	-13 -22	Quadrupole Split Peak
Oligoclase (An23)	11.7	-15	
Labradorite (An52)	11.7	-16	
Bytownite (An70)	11.7	-14	
Anorthite (An92)	11.7	-13	

[1] For quadrupolar nuclei apparent chemical shift changes with field strength. If peak is not split by second-order quadrupolar effects, value at 11.7 Tesla is essentially the isotropic chemical shift.

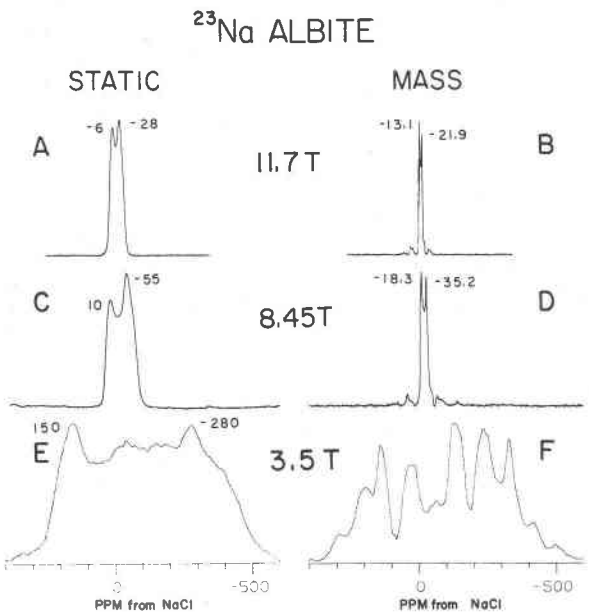

Fig. 10. ^{23}Na static and MASS NMR spectra of albite at 11.7, 8.45 and 3.5 Tesla. (A) 11.7 Tesla, static, 30 scans at 25 sec recycle time, 132 kHz spectral width, 3 μsec 90° pulse excitation, 4096 data points, 50 Hz linebroadening due to exponential multiplication. (B) 11.7 Tesla, 4.0 kHz MASS, 30 scans at 25 sec recycle time, 132 kHz spectral width, 3 μsec 90° pulse excitation, 8196 data points, 10 Hz linebroadening due to exponential multiplication. (C) 8.45 Tesla, static, 100 scans at 25 sec recycle time, 95 kHz spectral width, 3.5 μsec 90° pulse excitation, 4096 data points, 50 Hz linebroadening due to exponential multiplication. (D) 8.45 Tesla, 4.8 kHz MASS, 100 scans at 25 sec recycle time, 95 kHz spectral width, 3 μsec 90° pulse excitation, 8192 data points, 50 Hz linebroadening due to exponential multiplication. (E) 3.5 Tesla, static, 1000 scans at 25 sec recycle time, 39 kHz spectral width, 3.5 μsec 90° pulse excitation, 4096 data points, 100 Hz linebroadening due to exponential multiplication. (F) 3.5 Tesla, 3.5 kHz MASS, 1000 scans at 15 sec recycle time, 39 kHz spectral width, 3 μsec 90° pulse excitation, 4096 data points, 100 Hz linebroadening due to exponential multiplication.

The sodium-23 MASS NMR spectrum of sanidine (Fig. 8D) consists of a single broad peak at −21.2 ppm, which is slightly broader than those of albite and microcline perthite. The lack of a well resolved quadrupolar splitting for sanidine suggests to us, once again, that Al/Si disorder results in a range of sodium sites with different quadrupole coupling constants, asymmetry parameters, and/or chemical shifts. The presence of a split sodium-23 peak in alkali feldspars appears to be a good indicator of Al/Si ordering.

The sodium-23 MASS NMR spectra of the intermediate plagioclases (Fig. 9A–9D) all show single, relatively sharp centerband resonances in the range of −13.0 to −15.9 ppm, that are similar in shape and breadth to the sanidine spectrum. As for sanidine, this probably indicates a range of sites with different quadrupole coupling constants, asymmetry parameters, and/or isotropic chemical shifts. In the plagioclases, much of this is probably due to distortion of the sodium sites near the margins of albite and anorthite volumes. The relatively large spinning sidebands in these spectra, like the aluminum-27 NMR spectra of these same samples (Fig. 5), are probably due to the presence of magnetic impurities (Oldfield et al., 1983).

The sodium-23 NMR spectrum of albite glass (Fig. 8C) is very broad and featureless, again indicating sites with a range of quadrupole coupling constants, asymmetry parameters, and/or chemical shifts.

Summary and conclusions

The foregoing results demonstrate that MASS-VASS NMR spectroscopy complements well the other main, reasonably direct methods of investigating the structures of feldspars—single-crystal X-ray and neutron diffraction, electron diffraction, transmission electron microscopy (TEM) and single crystal NMR spectroscopy. Each of these methods has its strengths and its weaknesses. The particular strength of NMR spectroscopy is that in many

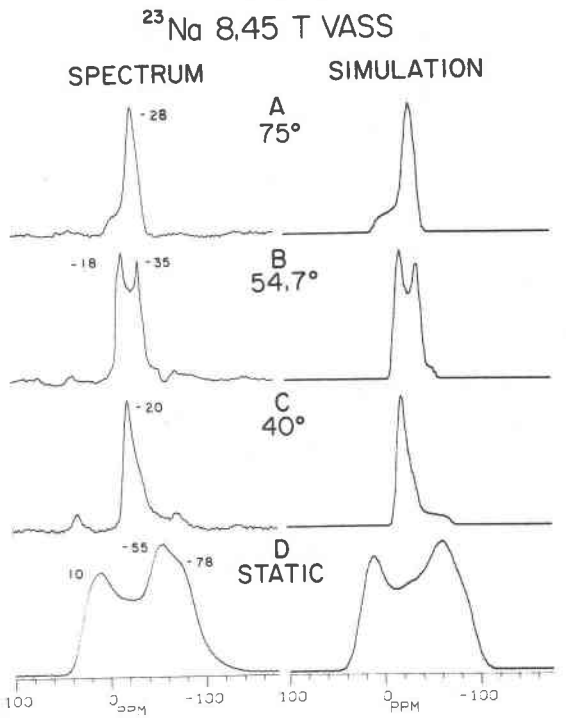

Fig. 11. 8.45 Tesla ^{23}Na static VASS NMR spectra and computer simulations of albite. All spectra: 5 kHz VASS, 50 scans, 25 sec recycle time, 14.2 kHz spectral width, 3 μsec 90° pulse excitation, 4096 data points, 50 Hz linebroadening due to exponential multiplication. The simulations assume a quadrupole coupling constant of 2.58 MHz and an asymmetry parameter of 0.25 and use 85 Hz linebroadening. (A) 75°, (B) 54.7° (magic angle), (C) 40°, (D) static.

instances it provides direct evidence about the electronic environment of individual kinds of atomic sites, even for those differing as little from one another as the T1m, T2m and T2o silicon sites in the triclinic alkali feldspars. Moreover, MASS-VASS NMR allows direct and easy comparison of sites in crystalline and noncrystalline materials. MASS-VASS NMR spectroscopy uses easily obtained powder samples whereas single-crystal NMR spectroscopy requires difficult-to-obtain, large, high-quality single crystals. The major limitations on MASS-VASS NMR samples are that they must be relatively free of paramagnetic impurities and that at least about 1–10 mg for sodium-23 and aluminum-27 and about 100–500 mg for silicon-29 must be available.

Although MASS-VASS NMR spectrometers currently are quite expensive and not numerous, this is likely to change for the better in the near future.

We now summarize for each type of material we have examined the results presented above. Again, we emphasize that while our interpretations are consistent with the available knowledge of and ideas about feldspar structure, they must at this time be considered tentative. Our interpretations of the intermediate plagioclase spectra are the most uncertain.

Alkali feldspars

Albite. Because it has an ordered and well-understood structure, the NMR spectra of low albite are the least ambiguous to interpret. The silicon-29 NMR spectrum has three well-resolved peaks of nearly the same intensity due to the three different silicon sites. The aluminum-27 NMR spectrum is a single relatively narrow peak, due to the one tetrahedral aluminum site. Both the silicon-29 and aluminum-27 data clearly support the high degree of Al/Si tetrahedral site ordering deduced by X-ray diffraction. The sodium-23 spectrum consists of a sharp, well-resolved doublet due to the second-order quadrupolar interaction, indicative of a rather asymmetric sodium site. All of these conclusions are consistent with the well-known structure of albite.

Microcline perthite. The spectra of this sample reflect the presence of both microcline and low albite. The silicon-29 NMR spectrum contains three peaks which are assignable to the three silicon sites in microcline, and two small peaks due to the small amount of intergrown albite. The third albite peak apparently underlies two of the microcline peaks. The aluminum-27 NMR spectrum of the perthite consists of a quadrupole split doublet from the microcline, and extra intensity due to the albite. The sodium-23 NMR spectrum consists of a quadrupolar split doublet, due to low albite, and a second component due to sodium in the microcline. The sodium site in the microcline is tentatively thought to be in an environment more symmetric than that in albite.

Cryptoperthite. The NMR spectra of the cryptoperthite (Spencer R) are consistent with partial Al/Si ordering and separation into potassium and sodium-rich volumes. The silicon-29 NMR spectrum is relatively well separated into a number of peaks. Three of these can be assigned to albite-like sites and to T1 and T2 sites in orthoclase (low sanidine). The resolution of the peaks is, however, not as clear as for the microcline perthite. There is only one aluminum-27 resonance, again indicating that neither phase has a composition approaching an end member. The sodium-23 NMR spectrum shows a somewhat smoothed out doublet due to quadrupolar splitting, again suggestive of at least enough Al/Si ordering to cause distortion of the sodium site. There is no sodium-23 resonance specifically assignable to the orthoclase.

Sanidine. Because sanidine is highly disordered, its spectra are also relatively easy to interpret. The two broad, poorly split silicon-29 NMR peaks are due to a range of silicon sites caused by Al/Si disorder in the T1 and T2 sites and to Or-Ab solid solution. These peaks cover the chemical shift range of the albite spectrum and indicate a continuum of electron distributions in $Q^4(0Al)$, $Q^4(1Al)$, $Q^4(2Al)$, and $Q^4(3Al)$ sites. The aluminum-27 NMR spectrum consists of a single peak which is broader than that of albite, also suggesting a range of aluminum environments in T1 and T2. The sodium-23 resonance is not split by quadrupolar effects, suggesting a range of sodium environments and probably a more symmetric environment.

Plagioclases

Anorthite. The silicon-29 NMR spectrum of synthetic anorthite consists of three $Q^4(4Al)$ peaks that are assignable to the eight silicon sites in anorthite plus a small peak that we assign to $Q^4(3Al)$ sites. The silicon-29 NMR spectrum of the natural anorthite (An_{92}), a phenocryst from Pacaya volcano (Guatamala), is similar but less well resolved. The aluminum-27 NMR spectrum of both anorthites are broad, with one well resolved peak, and a shoulder at less positive (more shielded) chemical shifts. MASS NMR is apparently not able to resolve the eight different aluminum sites. The sodium-23 spectrum of natural anorthite is discussed below along with those of the other intermediate plagioclases.

Intermediate plagioclases. The spectra of the intermediate plagioclases seem to be consistent with structural models involving *e*- and *I*-plagioclases with $Q^4(4Al)$ anorthite-like sites, $Q^4(1Al)$ and $Q^4(2Al)$ albite-like sites, and distorted equivalents of all three in strained regions where the albite-like and anorthite-like volumes meet. $Q^4(3Al)$ sites may also be present at the boundaries.

The silicon-29 NMR spectra of the oligoclase (An_{23}) and labradorite (An_{52}) exhibit three peaks that can be readily assigned to $Q^4(1Al)$ and $Q^4(2Al)$ sites in albite. The peaks do not all have the same height, as they do in low-albite. We have attributed the extra height in the -93 and -100 ppm range to deshielding of the albite-like sites and increased shielding of the anorthite-like sites caused by coherency strain of the silicon sites in *e*-plagioclase and, perhaps, to $Q^4(3Al)$ sites at the margins. In the

bytownite (An_{70}) the most shielded silicon peak is not present or is very small, perhaps suggesting that all of the albite-like volumes have strained silicon sites. The natural anorthite (An_{92}) has no peaks attributable to albite-like sites.

Peaks or shoulders in the silicon-29 NMR spectra which are attributable to anorthite-like sites increase in intensity with increasing An-content. For the oligoclase, there is only one shoulder at a relatively shielded chemical shift (−88 ppm), which we interpret as arising from strained $Q^4(4Al)$ anorthite-like sites. The peaks assignable to $Q^4(4Al)$ sites are larger in labradorite. We have attributed these peaks to anorthite-like sites in *e*-plagioclases. The peaks attributable to anorthite-like sites in the bytownite are very large. We attribute these peaks primarily to sites in *I*-anorthite, although some of the signal must come from sites in the *e*-plagioclase. As noted above, the silicon-29 NMR spectrum of the natural anorthite is similar to the synthetic anorthite, but less well resolved.

The aluminum-27 NMR spectra of the intermediate plagioclases consist of broad peaks that become more like that of anorthite with increasing An content.

The sodium-23 NMR spectra show single, unsplit peaks of about the same breadth as in sanidine. Because the silicon-29 NMR peaks indicate significant Al/Si order, we tentatively attribute the non-split sodium-23 resonances to variable amounts of strain of the sodium sites, which increases the range of electronic environments around sodium.

Glasses

The NMR spectra of the albite and anorthite glasses consist of single, essentially structureless peaks that are broader than the spectra of crystalline albite or anorthite. The silicon-29 resonances are broader by about 20 ppm. The aluminum-27 resonance for albite glass is about 20 ppm wider than that of low albite, whereas the aluminum-27 resonance of anorthite glass is only a few ppm wider than that of synthetic crystalline anorthite. This would seem to indicate a much larger increase in the range of aluminum sites in albite glass. The sodium-23 resonance of albite glass is about 20 ppm broader than that of low albite, again indicating a somewhat larger range of electric field gradients at the sodium sites in the glassy phase.

Acknowledgments

We wish to thank Drs. Glenn Buckley, David Stewart, and John Higgins, who supplied us with some of the samples and compositions, W. -H. Yang and Richard Oestrike for useful discussions, and an anonymous reviewer for many useful suggestions. This work was supported in part by the Solid-State Chemistry and Experimental and Theoretical Geochemistry Programs of the U.S. National Science Foundation (Grant DMR 8311339 and EAR 8207260 and 8408421) and in part by the U.S. National Institutes of Health, (Grant HL-19481) and has benefitted from facilities provided by the University of Illinois—National Science Foundation Regional NMR Instrumentation Facility. E. O. is a USPHS Research Career Development Awardee, 1979–1984.

References

Abragam, A. (1961) The Principles of Nuclear Magnetism. Clarendon Press, Oxford.

Andrew, E. R. (1971) The narrowing of NMR spectra of solids by high-speed specimen rotation and the resolution of chemical shift and spin multiplet structures for solids. Progress in NMR Spectroscopy, 8, 1–39.

Bollmann, W. and Nissen, H. -H. (1968) A study of optimal phase boundaries: the case of exsolved alkali feldspars. Acta Crystallographica, A24, 546–557.

Brown, B. E. and Bailey, S. W. (1964) The structure of maximum microcline. Acta Crystallographica, 17, 1391–1400.

Brun, E., Hartmann, P., Staub, H. H., Hafner, S., and Laves, F. (1960) Magnetische kernresonanz zur beobachtung des Al, Si-ordnungs/unordnungsgrades in einigen feldspäten. Zeitschrift für Kristallographie, 113, 65–76.

Farrar, T. C. and Becker, E. D. (1971) Pulse and Fourier Transform NMR: introduction to theory and methods. Academic Press, New York.

Fyfe, C. A., Gobbi, G. C., Klinowski, J., Thomas, J. M., and Ramdas, S. (1982) Resolving crystallographically distinct tetrahedral sites in silicalite and ZSM-5 by solid-state NMR. Nature, 296, 530–536.

Ganapathy, S., Schramm, S., and Oldfield, E. (1982) Variable-angle sample spinning high resolution NMR of solids. Journal of Chemical Physics, 77, 4360–4365.

Ghose, S. and Tsang, T. (1973) Structural dependence of quadrupole coupling constant e^2qQ/h for ^{27}Al and crystal field parameter D for Fe^{+3} in aluminosilicates. American Mineralogist, 58, 748–755.

Goldsmith, J. R. and Laves, F. (1955) Cation-order in anorthite ($CaAl_2Si_2O_8$) as revealed by gallium and germanium substitutions. Zeitschrift für Kristallographie, 106, 213–226.

Hafner, S. and Hartmann, P. (1964) Elektrische Feldgradienten und Sauerstoff-Polarisierbarkeit in Alkali-Feldspäten ($NaAlSi_3O_8$) und $KAlSi_3O_8$). Helvetica Physica Acta, 37, 348–360.

Hafner, S., Hartmann, P., and Laves, F. (1962) Magnetische Kernresonanz von Al^{27} in Adular. Zur Deutung der Adularstruktur. Schweizerische Mineralogische und Petrographische Mitteilungen, 42, 277–294.

Hafner, S. and Laves, F. (1963) Magnetische Kernresonanz von Al^{27} in einigen Orthoklasen. Schweizerische Mineralogische und Petrographische Mitteilungen, 43, 65–69.

Harlow, G. E. and Brown, G. E. (1980) Low albite: an X-ray and neutron diffraction study. American Mineralogist, 65, 986–995.

Higgins, J. B., and Woessner, D. E. (1982) ^{29}Si, ^{27}Al, and ^{23}Na spectra of framework silicates. (abstr.) Transactions of the American Geophysical Union (EOS), 63, 1139.

Kalus, C. K. (1978) Ph.D. Thesis, University of Munich. (Title unavailable.)

Klinowski, J., Ramdas, S., Thomas, J. M., Fyfe, C. A. and Hartman, J. S. (1982) A re-examination of Si, Al ordering in zeolites NaX and NaY. Journal of the Chemical Society, Faraday Transactions II, 78, 1025–1050.

Kundla, E., Samoson, A., and Lippmaa, E., (1981) High-resolution NMR of quadrupolar nuclei in rotating solids. Chemical Physics Letters, 83, 229–232.

Lippmaa, E., Mägi, M., Samoson, A., Engelhardt, G., and

Grimmer, A. -R. (1980) Structural studies of silicates by solid state high-resolution ^{29}Si NMR. Journal of the American Chemical Society, 102, 4889–4893.

Lippmaa, E., Mägi, M., Samoson, A., Tarmak, M., and Engelhardt, G. (1981) Investigation of the structure of zeolites by solid-state high-resolution ^{29}Si NMR spectroscopy. Journal of the American Chemical Society, 103, 4992–4996.

Loewenstein, W. (1954) The distribution of aluminum in the tetrahedra of silicates and aluminates. American Mineralogist, 39, 92–96.

McLaren, A. C. (1974) Transmission electron microscopy of the feldspars. In W. S. MacKenzie and J. Zussman, The Feldspars, p. 378–423. Manchester University Press.

Meadows, M. D., Smith, K. A., Kinsey, R. A., Rothgeb, T. M., Skarjune, R. P., and Oldfield, E. (1982) High-resolution solid-state NMR of quadrupolar nuclei. Proceedings of the National Academy of Science of the United States, 79, 1351–1355.

Megaw, H. D., Kempster, C. J. E., and Radoslovich, E. W. (1962) The structure of anorthite, $CaAl_2Si_2O_8$. II. Description and discussion. Acta Crystallographica 15, 1017–1035.

Muir, I. D. and J. V. Smith (1956) Crystallisation of feldspars in larvikites. Zeitschrift für Kristallographie, 107, 182–195.

Müller, D., Gessner, W., Behrens, H. J., and Scheler G. (1981) Determination of the aluminum coordination in aluminum-oxygen compounds by solid-state high-resolution ^{27}Al NMR. Chemical Physics Letters, 79, 59–62.

Mysen, B. O., Virgo, D., and Seifert, F. A. (1982) The structure of silicate melts: implications of chemical and physical properties of natural magma. Reviews of Geophysics and the Space Physics, 20, 353–383.

Oftedahl, C. (1948) Studies on the igneous rock complex of the Oslo region. IX. The feldspars. Skrifter utgit av Det Norske Videnskaps-Akademi i Oslo I. Mathematisk-Naturidenskapellig Klasse. 1948. No. 3. Naturvidensk Kl. 3.

Oldfield, E., Kinsey, R. A., Smith, K. A., Nichols, J. A., and Kirkpatrick, R. J. (1983) High-resolution NMR of inorganic solids. Influence of magnetic centers on magic-angle sample-spinning lineshapes in some natural alumino silicates. Journal of Magnetic Resonance, 51, 325–327.

Ribbe, P. H., (1983) Feldspar Mineralogy, Vol. 2. Reviews in Mineralogy, 2nd Edition. Mineralogical Society of America, Washington, D.C.

Schramm, S. E. and Oldfield, E. (1982) High resolution solid state NMR of quadrupolar nuclei: quadrupole induced shifts in variable-angle sample spinning of a borosilicate glass. Journal of the Chemical Society, Chemical Communications, 980–81.

Smith, J. V. (1974) Feldspar Minerals, volume 1. Springer-Verlag, New York.

Smith, J. V. and Blackwell C. S. (1983) Nuclear magnetic resonance of silica polymorphs. Nature, 223–225.

Smith, J. V., Blackwell, C. S., and Hovis, G. L. (1984) Nuclear magnetic resonance of albite-microcline series. Nature, 309, 140–142.

Smith, J. V. and Muir, I. D. (1958) The reaction sequence in larvikite feldspars. Zeitschrift für Kristallographie, 110, 11–20.

Smith, K. A., Kirkpatrick, R. J., Oldfield, E., and Henderson, D. M. (1983) High-resolution silicon-29 nuclear magnetic resonance spectroscopic study of rock forming silicates. American Mineralogist, 68, 1206–1215.

Spencer, E. (1937) The potash-soda feldspars I. Thermal stability. Mineralogical Magazine 24, 453–494.

Staehli, J. L. and Brinkmann, D. (1974a) A nuclear magnetic resonance study of the phase transition in anorthite, $CaAl_2Si_2O_8$. Zeitschrift für Kristallographie, 140, 360–373.

Staehli, J. L. and Brinkmann, D. (1974b) Assignment and structural dependence of electric field gradients in anorthite and simple field gradient calculations in some aluminosilicates. Zeitschrift für Kristallographie, 140, 374–392.

Stewart, D. B. and Wright, T. L. (1974) Al/Si order and symmetry of natural alkali feldspars and the relationship of strained cell parameters to bulk composition. Bulletin de la Société Française de Mineralogie et de Cristallographie, 97, 356–377.

Taylor, M., and Brown, G. E. (1979) Structure of mineral glasses. I. the feldspar glasses $NaAlSi_3O_8$, $KAlSi_3O_8$, $CaAl_2Si_2O_8$. Geochimica et Cosmochimica Acta, 43, 61–77.

Wainwright, J. E., and Starkey, J. (1971) A refinement of the structure of anorthite. Zeitschrift für Kristallographie, 133, 75–84.

Manuscript received, October 26, 1983;
accepted for publication, September 4, 1984.